High electron gain from single-walled carbon nanotubes stimulated by interaction with an electron beam

Mario Michan, Parham Yaghoobi, Bertin Wong, and Alireza Nojeh*

Department of Electrical and Computer Engineering, The University of British Columbia, Vancouver, British Columbia, Canada V6T 1Z4

(Received 17 September 2009; revised manuscript received 2 April 2010; published 27 May 2010)

Carbon nanotubes are excellent electron emitters due to their sharp geometry and high electrical conductivity and mechanical stability. It has previously been shown that an electron beam hitting the tip of a nanotube biased near the threshold of field-emission can stimulate the emission of a large number of electrons from the nanotube tip. Here we present a detailed characterization of this so-called electron-stimulated field-emission phenomenon. Electron gains of up to 2300 were obtained. We also discuss possible direct and indirect electron-nanotube interaction mechanisms responsible for this high gain. This effect has a good potential for vacuum nanoelectronic applications.

DOI: 10.1103/PhysRevB.81.195438 PACS number(s): 79.20.Kz, 79.70.+q, 79.90.+b, 73.90.+f

I. INTRODUCTION

Single-walled carbon nanotubes (SWNTs) are tubular structures made of carbon atoms in a honeycomb lattice that can be thought of as rolled graphene. They have diameters of around 1 nm and can be as long as a few centimeters. SWNTs show very high strength, mechanical stability, and excellent electrical conductivity. Additionally, they are excellent electron field-emitters. Pioneering work on field-emission from nanotubes was done in the mid 1990s (Refs. 1–3) and many subsequent works have further examined their interesting field-emission behavior.[4,5] Several review articles have been written on the topic, including an early review by Bonard *et al.*[6] and more recent ones.[7,8] Field-emission is a process whereby electrons are extracted from a surface under a high external electric field. The process is due to quantum tunneling and typically produces a more narrow distribution of electron energies and a more localized emission area than thermionic emission where the electrons are excited by high temperatures.

In one particular experiment, the primary beam of a scanning electron microscope (SEM) was observed to trigger field-emission from a biased SWNT lying on an insulating substrate.[9,10] This effect was called stimulated field-emission (SFE) since the bias applied to the carbon nanotube (CNT) was not strong enough to cause field-emission by itself; an additional stimulation—the SEM's primary electron beam—was required to initiate the emission process. This emission happened only when the scanning primary beam hit the nanotube tip. Therefore, it appeared on the SEM image as a bright spot—the result of a large number of emitted electrons saturating the secondary electron detector at the moment when the primary beam was on the tip of the nanotube. Stimulated field-emission has also been observed from multi-walled carbon nanotubes interacting with a SEM beam.[11]

As will be discussed in detail in the present report, SFE shows a high electron gain. This is interesting since such a device could form the basis of a nanoscale current-controlled vacuum transistor, an electron multiplier, or a highly localized electron detector. The stimulating mechanism was believed to be at least partially the direct interaction of the primary beam electrons with the nanotube tip. Such an interaction was investigated using first-principles calculations and it was observed that an electron entering the nanotube tip region raises the orbital energies significantly, making their occupying electrons more susceptible to tunneling out of the nanotube.[12] In this paper, we further characterize the behavior of these devices, in particular, by measuring the electron gain under different conditions and attempt to shed further light on the possible interaction mechanisms at work.

II. DEVICE STRUCTURE AND FABRICATION

In order to characterize this phenomenon several experiments in multiple devices were performed. Figure 1 shows a schematic of a typical device and its SEM image. The SWNT is lying on a SiO_2 substrate. The substrate provides mechanical support and a mechanism for cooling down by heat exchange during emission (nanotubes on a substrate have been observed to enable the passage of higher current compared to suspended ones due to thermal relaxation through the substrate[13]). The devices have integrated cathode and anode electrodes. This arrangement, given the small distance between the electrodes, allows us to generate the necessary electric fields using a small bias voltage. In this way the operation of the SEM and the primary beam trajectory are not disturbed. The devices were fabricated using standard microfabrication processes (lithography, metal deposition and lift-off) to pattern the electrodes (molybdenum) and catalyst islands. Nanotubes were grown using chemical vapor deposition. A more detailed description of this process can be found in Ref. 10.

III. EXPERIMENTS

The experiments were performed in a Philips 525M SEM, which was additionally equipped with electrical feedthroughs to allow the *in situ* biasing of the nanotubes and current measurements. A custom-designed sample holder was made with suitable current guards to reduce parasitics and leakage currents. A Keithley 6517A electrometer was used as voltage source and current meter. This instrument, with a 1×10^{-15} A resolution, provided sufficient accuracy for the measurements. This electrometer was interfaced with

 ©2010 The American Physical Society

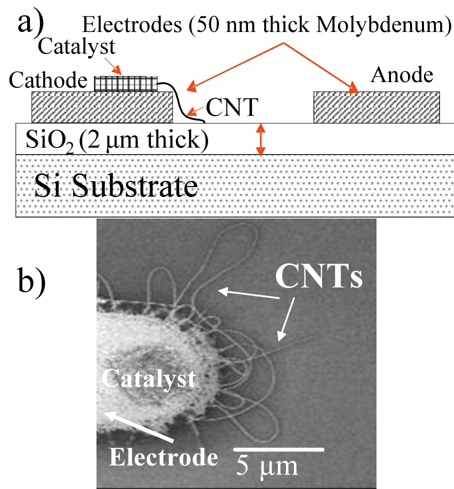

FIG. 1. (Color online) (a) Cross-sectional schematic view of the device structure. (b) SEM image of a device (top view). The molybdenum cathode is visible on the left with a catalyst island and several nanotubes a few micrometer long each attached to it and lying on the SiO_2 substrate. The anode is on the right side (not in the field of view here) at approximately 30 μm from the nanotubes.

a computer in order to record voltage and current as a function of time. Given the small magnitude of the currents measured, we had to improve the signal-to-noise ratio by averaging several readings, typically from 10 to 100, and by choosing a suitable analog-to-digital converter integration time in the order of 2 ms. This strategy improves the signal-to-noise ratio but at the same time decreases the maximum sampling rate possible. Figure 2 shows the schematic of the experimental apparatus.

During a typical experiment the device under test was initially imaged with the SEM and the primary beam current was measured with a Faraday cup. The anode (extractor) was

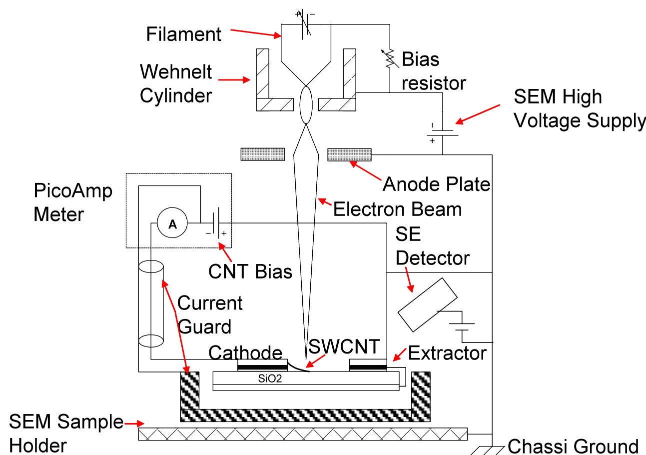

FIG. 2. (Color online) Schematic of the experimental apparatus with the device under test. The diagram shows the Keithley 6517A electrometer, which was used as voltage source and current meter, the device with CNTs and integrated electrodes, and the Philips 525 SEM with the high-energy electron beam and the secondary electron detector. Additionally the current guard circuit and common ground are shown.

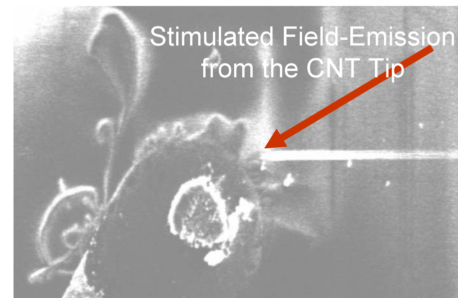

FIG. 3. (Color online) SEM image of an SFE event obtained from the device shown in Fig. 1 (The image is rotated by ~45° compared to Fig. 1). SFE started when the electron beam hit the tip of the nanotube and continued for about 2 ms. The bright stripe in the image is caused by emitted electrons saturating the secondary electron detector as the primary beam scans beyond the nanotube tip for that time. This SFE event happened with a primary beam energy of 5 keV, spot size of 5 nm and primary beam current of 0.8 pA. The maximum emission current measured in this experiment was 12.2 pA.

held at ground potential and the cathode (the electrode where the nanotube was attached) was biased negatively. Any emission or leakage current through the cathode was measured with the current meter. The bias was then increased slowly up to just before the threshold of regular field-emission. At this bias, stimulated field-emission could be observed as a bright spot on the nanotube tip (Fig. 3). (Further increasing the bias into the regular field-emission regime would, of course, lead to the SEM image being washed out since the spontaneously field-emitted electrons from the nanotube tip would flood the secondary electron detector regardless of the position of the primary beam.) As can be seen in Fig. 3, often the emission would continue for some time after the primary beam had swept past the nanotube tip, leading to a streak on the image. The bright spot and line are due to secondary electron detector saturation by the portion of SFE electrons that escape the device anode and fly to the detector. The stimulated emission current was recorded as peaks that agreed with the timing of the scanning primary beam hitting the nanotube tip (Fig. 4). This SFE event happened with a primary beam energy of 5 keV, spot size of 5 nm, and primary beam current of 0.8 pA. The maximum emission current measured in this experiment was 12.2 pA.

The experiments were performed under different conditions where several of the parameters that could potentially play a role in the emission current were varied. The scan period can be adjusted in the SEM as well as the primary beam energy and spot size. The applied bias varied from device to device (different geometries) between −150 and −170 V. Given the anode-cathode distance of 32.5 μm this corresponds to average applied electric fields in the range of 4.6–5.2 V/μm along the nanotube, which are around the threshold of field-emission for carbon nanotubes. Obviously, due to the high aspect ratio of the nanotubes, the field at the nanotube tip is enhanced hundreds of times compared to the applied field.[14,15] As will be further discussed, based on our simulations, this effective field at the tip of the nanotube was almost the same in all devices during SFE.

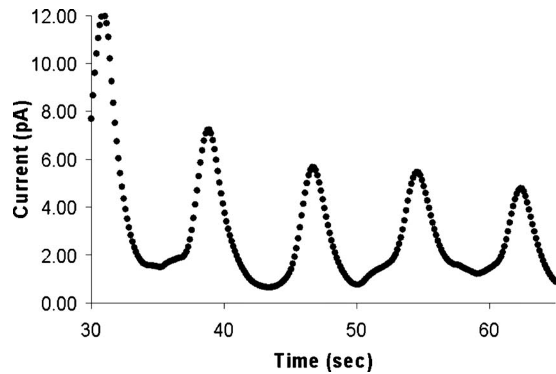

FIG. 4. Cathode current during an SFE experiment with a 5 keV/5 nm spot primary beam scanning at 0.032 s per line and 250 lines per frame. The SFE current peaks occur every 8 s, which correlates with the primary beam scanning over the tip of the nanotube.

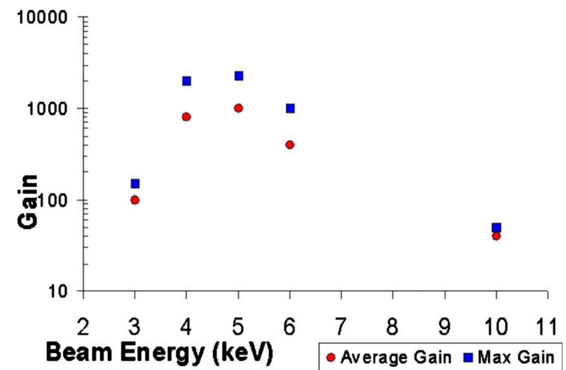

FIG. 5. (Color online) Measured maximum electron gain for a single SFE event and average gain for SFE at different primary beam energies. The electron gain is calculated as the ratio of the number of electrons passing through the cathode in the circuit of Fig. 2 per the number of primary beam electrons reaching the sample during one interaction cycle.

IV. RESULTS

Stimulated field-emission was clearly observed at primary beam energies of 3, 4, 5, 6, and 10 keV. It was not observed at 1, 2, and 15 keV, indicating that either there was no SFE or it was weak and obscured by noise. Experiments performed on different devices showed some variance in SFE current amplitudes (with a few of the devices showing no field emission at all). However, at any given primary beam energy most devices performed similarly and the main difference between different energies was the amplitude of the SFE current. Figure 4 is an example of the current measurements obtained as a function of time. For this particular experiment the primary beam energy was 5 keV and it hit the nanotube tip every 8 s. This experiment produced a very clean signal. The variations in current peaks are believed to be due to instabilities (and the gradual deterioration of the nanotube tip) partially because of the poor vacuum conditions in the SEM chamber. This will be discussed further.

The electron gain was calculated as the ratio of the number of electrons passing through the cathode in the circuit of Fig. 2 per the number of primary beam electrons reaching the sample during one interaction cycle. Figure 5 shows the average gain calculated from all the SFE peaks during an experiment and the maximum gain obtained in a single SFE event, both as a function of primary beam energy. The global maximum gain obtained was for a single event in an experiment at 5 keV and was 2300. The average gain at this energy is $\sim$1000. It can be observed that the gain increases as the primary beam energy is increased from 3 to 5 keV where it reaches a maximum. As the beam energy is further increased the gain decreases to a minimum average value of 40 at 10 keV. At 3 and 10 keV the maximum gain is very close to the average gain (150 and 100 for 3 keV and 50 and 40 for 10 keV). SFE at 5 keV showed the largest difference between maximum and average gain; the SFE current peaks were very large and clear at this primary beam energy, but their amplitude decreased rapidly as the experiment progressed. The effects of line scan period and beam spot size were also characterized for the primary beam energies investigated. The scan period was varied from 2 to 32 ms per line, and it did not affect the current gain. Faster scanning rates could not be investigated due to the limitations of our experimental data acquisition setup. The primary beam spot size was varied from 5 to 50 nm and it also did not cause any appreciable change in the measured gain.

The obtained gain value is based on the cathode current measured by the electrometer and is composed of the SFE current, as well as possible leakage currents between the biased electrodes through the oxide surface. Leakage currents were measured to be approximately 0.45–1.50 pA: they were comparable to the primary beam current and much smaller than the SFE current. Therefore, their contribution is negligible in the gain calculation. The primary beam current was measured independently with a Faraday cup that suppresses the effect of reflected electrons. This current changes according to the adjustment of the SEM for imaging and in our various experiments it ranged from 0.45 to 2.00 pA.

V. ANALYSIS AND DISCUSSION

An important factor that needs to be considered when calculating the gain is the actual interaction area of the primary beam and the nanotube. Most of the time that the primary beam is scanning the substrate, it is not interacting directly with the CNT tip. Nevertheless, the interaction area could potentially be much larger than the area of the nanotube tip due to the spreading of the beam in the substrate.

This area can be measured using the digitally captured SEM images of SFE events: since the secondary electron detector records values at every point as the primary beam moves, and a percentage of SFE electrons are always captured by it, the SEM image provides a good measurement tool for the interaction area. Although the accuracy is limited by the pixel resolution, it is better than what the sampling rate of the electrometer allows. Figure 6(a) is a zoomed-in image of the SFE spot of Fig. 3, and Fig. 6(b) shows the pixel intensity as extracted from the image file. (As mentioned before, the horizontal streaks indicate that the emission continues for some time—in this case about 2 ms—after

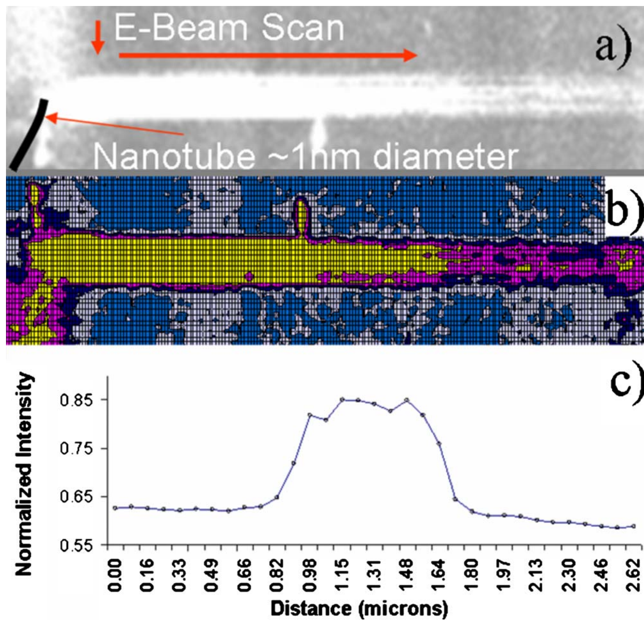

FIG. 6. (Color online) (a) Zoomed-in image of the SFE spot of Fig. 3 with the primary beam scanning direction and emitting nanotube position as indicated. (b) Pixel intensity map extracted from image. (c) Average intensity of each row as a function of distance from the top edge of the SEM image shown in (a).

the primary beam has swept past the nanotube tip; a possible explanation for this will be discussed later.) The graph in Fig. 6(c) is the average pixel intensity vs distance from the bottom edge of the image (the value at each point is the average intensity of all the pixels in the corresponding row).

The emission current and, as a result, the percentage of electrons captured by the detector increased as the primary beam approached the nanotube, although the plot in Fig. 6(c) is truncated due to the saturation of the secondary electron detector. In this example each pixel on the digitized image was 82×82 nm^2 and, as can be seen in Fig. 6, the interaction area has a radius of approximately 450 nm. In other words, SFE started when the 5-nm-diameter primary beam was as far as 450 nm from the ~1-nm-diameter CNT. This distance is too large for direct interaction of the primary beam electrons and the CNT tip. This indicates that there is some indirect interaction at play. One possibility is that the oxide layer acts as an intermediary to enable this long-range interaction. Below we further investigate this possibility.

When the primary beam impinges on the SiO_2 layer, it produces reflected electrons that could escape the surface some distance away from the primary beam. These electrons could potentially be interacting with the nanotube and leading to SFE. In order to verify this hypothesis Monte Carlo simulations of the interaction of the primary beam electrons and the SiO_2 layer were performed using the software CASINO.[16] Figure 7 shows the electron trajectories for a primary beam energy of 5 keV and a spot size of 5 nm. The penetration depth and radius of the interaction can be observed.

From the figure it is evident that backscattered electrons (BEs) and, as a consequence, secondary electrons (SEs) can be reflected from the surface as far as about 480 nm from the

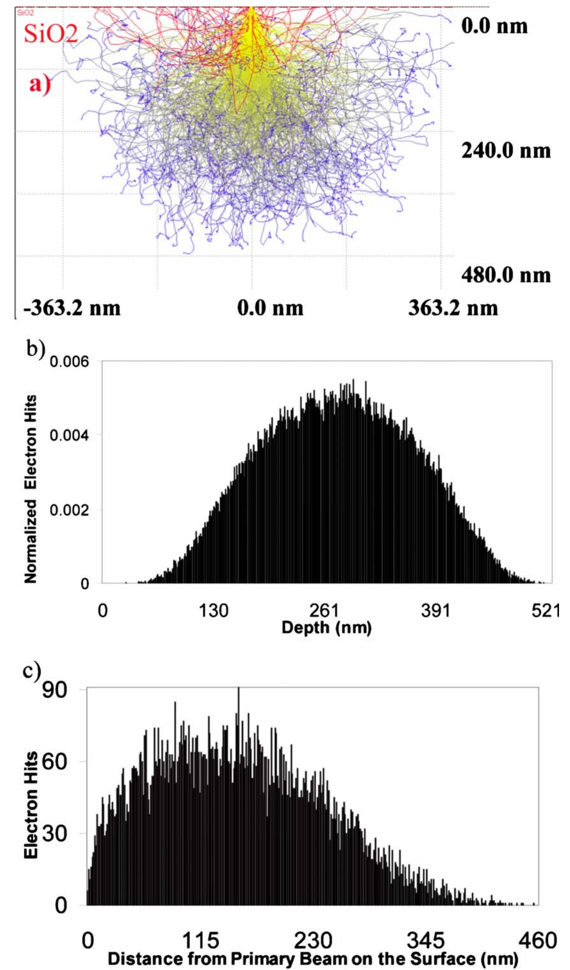

FIG. 7. (Color online) (a) Electron trajectories calculated with a Monte Carlo simulation of the primary beam interaction with the SiO_2 substrate using the program CASINO (Ref. 16). The primary beam energy is 5 keV and the spot size 5 nm; 100 000 electrons were used in the simulation. (b) Distribution of electrons as a function of penetration depth into the substrate. The maximum depth is ~520 nm. (c) Distribution of backscattered electrons (energy greater than 50 eV) as a function of distance from the primary beam on the substrate surface.

primary beam location. This is consistent with the observation that the interaction seems to occur as far as 450 nm and provides a possible explanation for the size of the interaction area observed.

Other interaction mechanisms are not necessarily ruled out. An important such mechanism could be the charging of the oxide region around the nanotube tip as a result of irradiation by the primary beam, which could significantly affect the local electric field. For instance, not all of the primary beam charge is reflected and some of it will stay in the substrate. The BEs will also create more SEs as they move through the lattice and some of those SEs generated below the escape depth will charge the surface. The escape depth of SEs for SiO_2 is between 10 and 20 nm (Ref. 17) and charge will most likely accumulate below this depth in a region with a radius of about 480 nm around the primary beam for the 5 keV case. Oxide charging will affect the electric field at the

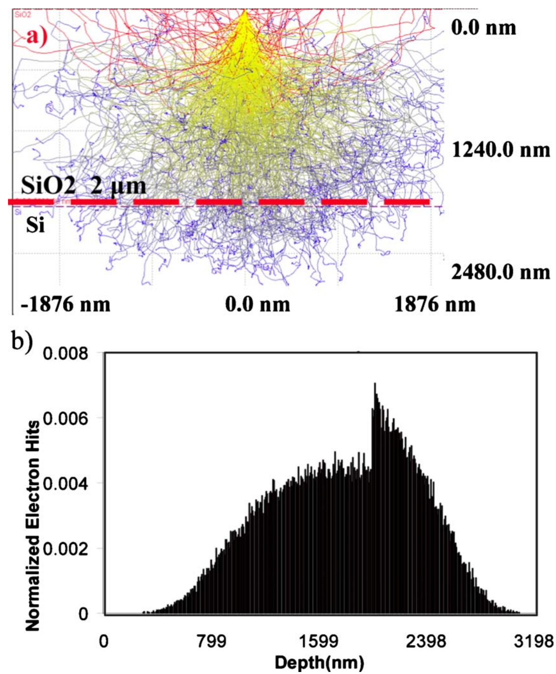

FIG. 8. (Color online) (a) Electron trajectories calculated with a Monte Carlo simulation of 100 000 electrons at 15 keV and 5 nm spot size and impinging on a 2 μm SiO_2 layer on a Si substrate. (b) Distribution of electrons as a function of penetration depth into the SiO_2 layer. The large peak corresponds to the SiO_2-Si interface.

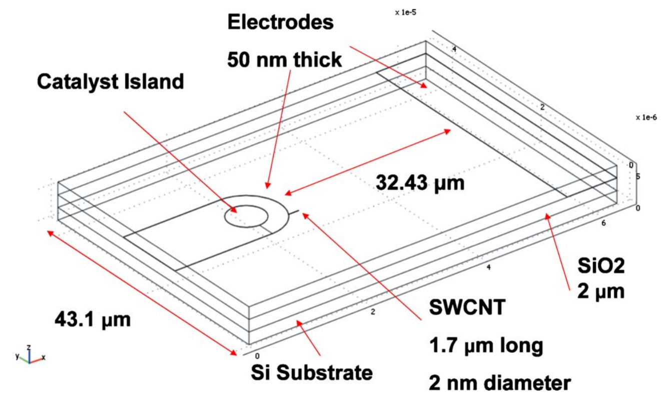

FIG. 9. (Color online) A model of one of the experimental devices used to simulate the electric field at the tip of the nanotube. The model closely matches the dimensions and materials used in the actual devices.

tip of the nanotube, potentially assisting in electron emission. An observation that supports that oxide charging is playing an important role is that, as mentioned before, SFE is pervasive. Figures 3 and 6 show bright streaks that extend as far as 2 ms after the primary beam has swept past the initial emission spot. An estimate of the oxide discharge *RC* constant indicates that the discharge time is in the order of a few milliseconds. Furthermore, SFE was not observed for a 15 keV primary beam. Monte Carlo simulations of the 15 keV beam (Fig. 8) show that the penetration depth for this energy is larger than 2 μm, which is the thickness of the oxide layer over a highly doped, low-resistivity silicon substrate. Therefore, at this energy, a continuous discharge path to the ground exists through the so-called electron-beam-induced current and no charging occurs in the dielectric and, consequently, no SFE due to oxide charging.

In order to further investigate the effect of dielectric charging and separate it from direct interaction of electrons (primary or secondary) with the nanotube tip, experiments were also performed with a different type of device with an oxide thickness of 400 nm. At this thickness no substrate charging should occur beyond a primary beam energy of 4.2 keV and therefore no SFE caused by charging. Nevertheless, SFE was observed in these devices at 5 keV and even 10 keV where no charging should occur. At 5 keV the primary beam is already reaching the silicon substrate inducing currents and cancelling any surface charging (see simulation in Fig. 7). The fact that no charging was happening was confirmed by zooming in and out of the image in the SEM and observing the brightness of the substrate (no dark charging boxes were observed). Similarly, at 10 keV more than 90% of the electrons will punch through the oxide layer and the surface charging will be zero or even positive. Interestingly, in these cases the SFE peak current recorded was not as large as in the previous experiments (where there was charging). Furthermore, SFE was not pervasive like in those cases. The maximum gain calculated for these devices was ~20 at 5 keV and the average gain was ~10. The main stimulating process in this case is believed to be direct interaction of the CNT with the primary beam electrons or secondary electrons. A possible mechanism for such direct interaction is the rise in the nanotube tip energy levels (effective reduction in work function) due to the external electron placed inside the nanotube as investigated in Ref. 12. Another interesting point is that the interaction area observed in these cases is not as large as the surface area of BE escape estimated by Monte Carlo simulations. For instance, for the 10 keV case, the radius of this area is as large as a 1.3 μm. However, the SFE peaks observed indicate a much smaller interaction area with a radius of approximately 150 nm. Nonetheless, similarly to the cases where oxide charging exists, as the beam energy is increased the electron gain decreases and SFE disappears at about 15 keV. This is also consistent with the direct interaction mechanism proposed in Ref. 12: higher-energy electrons spend less time in the nanotube. Thus, the resulting rise in nanotube energy levels will also exist for a shorter period of time (for instance, ~0.01 fs for 15 keV electrons passing through a nanotube with a 1 nm diameter perpendicular to it), which may not be sufficient for the emission of other electrons from the nanotube.

In order to further quantify the effect of substrate charging a simulation of the electrostatic field in the device was performed using the electrostatics module of the software COMSOL MULTIPHYSICS. Figure 9 shows the model and Fig. 10 a comparison of the model with an actual device. The model dimensions were chosen in a way so as to closely mimic one of the actual tested devices. The nanotube was modeled as a hollow perfect conductor with a width of 2 nm and length of 1.7 μm. Values of 12.1 and 4.2, respectively, were chosen for the relative permittivity of silicon and silicon dioxide (as given by the COMSOL database). A total of approximately 20 000 mesh points were used for the simulation. Figure 10

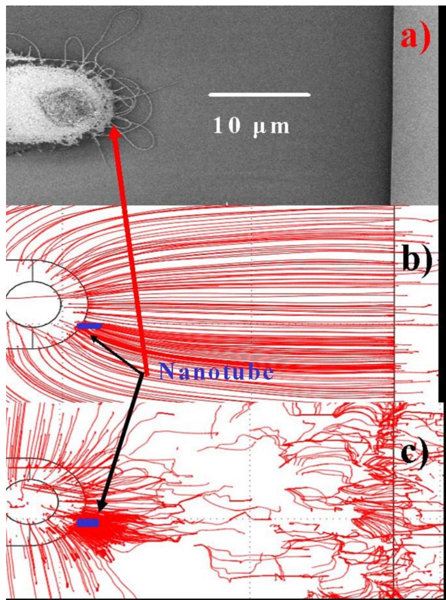

FIG. 10. (Color online) (a) SEM image of the device. Top view of the calculated electric field distribution without any substrate charging: (b) without a ground plane and (c) with a ground plane. As expected, the image shows a higher electric field flux (higher effective electric field) at the tip of the nanotube. The value of the field at the nanotube tip is comparable in both cases.

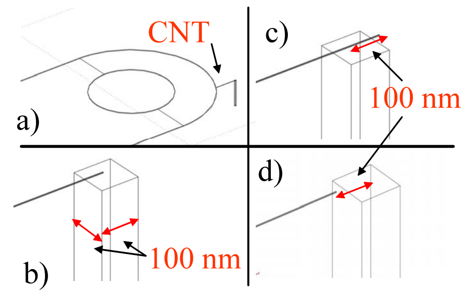

FIG. 11. (Color online) (a) Schematic of the model showing the cathode electrode with a nanotube and the charge pixel directly below the tip. The charge pixel is 100×100 nm^2. (b) Charge pixel centered at the CNT tip position. (c) Charge pixel 100 nm before the tip of the nanotube. (d) Charge pixel 100 nm in front of the nanotube tip.

shows the distribution of the field in this device without any oxide charging.

The ground connection to the silicon substrate is done through a thin oxide layer on the back of the silicon substrate and occasional contamination. Two extreme cases for this contact can be considered: zero and infinite resistance. In the former case, the silicon substrate would be fully grounded and at the same potential as the anode. In the latter, it would be a floating conducting plane. The simulations were performed for both cases (Fig. 10). However, both simulations give field values within the same order of magnitude and lead to the same qualitative conclusions.

In the next step, the oxide charge was calculated as a function of the primary beam energy and current with a MATLAB script using the SiO_2 backscattered and secondary electron yield coefficients published by Joy.[18] For a detailed description of the calculation see appendix or Refs. 17, 19, and 20. Then, the electric field distribution was simulated again for the device, but this time also including the effect of the dielectric charge. Figure 11 shows a volume the size of a charge pixel that was moved around the device in the model. This pixel was charged with the value calculated above (-8 C/m^3). The pixel is 100×100 nm^2 in size and it represents the charging area caused by the primary beam as it scans the device. In the figure, three different positions are shown: the pixel centered below the CNT tip, 100 nm before the tip, and 100 nm after the tip.

The reason for using a 100×100 nm^2 charge pixel instead of the full interaction area discussed earlier is that the charging electrons are not distributed uniformly over the whole interaction area, but should follow a spatial distribution similar to that of the secondary electrons. In this distribution the charge density is highest at the center and most of the charge will be concentrated within about a 50 nm radius from the center. The SE distribution has been previously described in the literature.[17] Since according to this distribution most of the charge will be concentrated within a 50 nm radius, a charge pixel size of 100×100 nm^2 (with uniform distribution for simplicity) was used for the simulation. Although this size and shape may seem somewhat arbitrary, here we are using them to gain a qualitative, rather than exact quantitative, insight into the effect of oxide charging on electron emission.

In Fig. 10 we saw the electric field distribution in a device without any surface charging, under an applied bias of 150 V. The field at the nanotube tip was found to be approximately 2 V/Å (typical for field-emission threshold), indicating a field enhancement factor (which we define as the ratio of the field at the nanotube tip to the field at the same location when no nanotube is included in the simulation) of approximately 100. On the other hand, the field enhancement when the substrate directly below the nanotube tip was negatively charged [corresponding to Fig. 11(b)] was calculated to increase 12 times, leading to an enhancement of 1200. This implies a tremendously high emission current. Of course such a high value will not be reached in practice since electron emission will happen long before this point and the charging dynamics will change. Obviously the reality of the interaction is more complex than this static charging model. However, the model provides insight into the strength of this oxide charging mechanism. When the charged pixel was placed 100 nm behind the tip of the CNT under the CNT body [as in Fig. 11(c)], the field enhancement decreased to about 500. This is five times the field enhancement without surface charge. When the charge pixel was moved 100 nm in front of the tip [Fig. 11(d)], field enhancement was reduced to 400, namely, four times the value without surface charging. (The values mentioned above are averages from the two cases simulated, namely, with the silicon substrate fully grounded and with the substrate as a floating, conducting plane.)

When the charge pixel was placed at any other location, more than 200 nm away from the CNT, it would actually reduce the field enhancement at the nanotube tip. The worst

case found reduced it to 50, namely, half of the field enhancement value with no charge at all. This happened when the charge pixel was placed at 1 μm directly in front of the CNT. The same value was obtained when the entire substrate was uniformly charged. Since tunneling and, therefore, the electron emission current, are exponentially dependent on the field, these drastic variations in local field because of the action of the primary beam in charging the oxide provide a possible explanation for the observed peaks in SFE current and the high gain obtained. Note that the presence of other nanotubes and defects in a real device would affect the field-enhancement factor, however, such effects do not change the qualitative discussion presented here. Other types of mechanisms such as interactions with plasmons, Auger electrons, and x rays may also play a role. Some of these mechanisms have been previously examined by Kasumov *et al.*[21] Another possible effect could be the enhanced adsorption of residual gases on the nanotube tip that could lead to increased field-emission current.[22,23]

It is worth re-emphasizing that in a typical experiment, the first SFE peaks obtained are usually quite large, but they gradually decrease in intensity as the primary beam hits the nanotube tip over and over again (Fig. 4). Given the energy range of the primary electrons, it is unlikely that any direct damage to the tip is caused by the beam. Such damage typically occurs at beam energies beyond 100 keV.[24] However, under the poor vacuum conditions of the experiment, it is expected that the electrostatic deposition of particles or electron-beam-induced amorphous carbon deposition on the nanotube tip would gradually deteriorate the tip's sharp structure. Observations of a deformed nanotube tip at the end of the experiments (not shown here) support this explanation. This would gradually decrease the emission current and eventually lead to the destruction of the device. So far the damage in all our tested devices has been permanent and no further SFE has been obtained from any device once it has stopped functioning in a particular experiment. Figure 12 is the SFE current in a device when a 5 keV primary beam was kept in line scan mode, that is scanning back and forth along a single line, passing through the nanotube tip. The line scan period was 32 ms. The experiment was repeated two consecutive times as it can be seen in Fig. 12, each time for about 10 s before the beam was slowly moved away from the nanotube. In this configuration the beam hits the nanotube once every 32 ms. Every data point corresponds to the average current for a few line scans. The current decreased over time (from the point at about 104 s in Fig. 12 to 111 s). In the second stimulation (starting at ~122 s), the current began from the last value recorded during the first stimulation and continued decreasing. Notice that in Fig. 4 we have shown the current readings as the beam was scanning the sample at 32 ms per line and the frame consisted of 250 lines. According to the scanning time, the SFE occurred every 8 s. In that case the current peaks also decreased with time.

Finally, a note on the SEM imaging of nanotubes is in order: given the small interaction area of a single-walled carbon nanotube with the primary beam, it has been rather surprising that SWNTs are so readily observable in an SEM. The fact that, as revealed by the present work, the primary beam seems to have both strong direct interaction with the nanotubes, as well as strong interaction with them through the substrate (consistent with previous reports such as that of Kasumov *et al.*[21]), is thus relevant to nanotube electron microscopy in general.

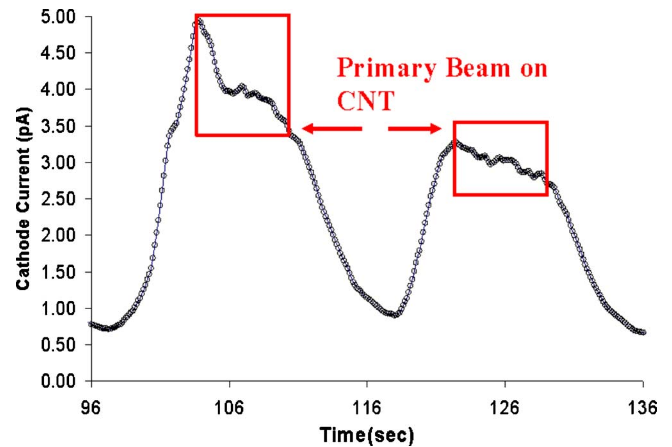

FIG. 12. (Color online) SFE with a 5 keV primary beam in line scan (32 ms per line) along a line passing through the nanotube tip. The nanotube tip was being hit every 32 ms by the primary beam. Every data point corresponds to the average current for a few line scans. The beam was slowly moved toward the nanotube at time ~100 s and away starting at approximately time 111 s. It was brought back over the nanotube starting at approximately 118 s and away at 130 s.

VI. SUMMARY

Two interaction mechanisms, namely, direct interaction of primary electrons and oxide charging seem to play a role in electron-stimulated field-emission. Direct electron-nanotube interactions seem to account for lower electron gains, in the order of 10–20. Substrate charging, on the other hand, appears to account for much larger gains. In the 5 keV experiment an average gain of approximately 1000 was calculated and this was the result of both types of interactions. The maximum gain obtained in our experiments was 2300. Other mechanisms such as interactions through plasmons, Auger electrons and x rays, as well as enhanced adsorption of residual gases, may also play a role, but we have not investigated those here.

Regardless of the actual interaction mechanisms behind this effect, the high values of gain could find a use in applications such as vacuum nanotransistors, electron multipliers or detectors with high spatial resolution. The gain of such devices could be improved by the proper choice of dielectric and device geometry. However, more work is needed in order to make such applications a reality. For example, knowledge of the energy distribution of the emitted electrons can provide valuable additional information on the nanoscale interactions. Also experiments in ultrahigh vacuum may provide more clear readings of SFE and more insight into the reasons for emission decay. Additionally, experiments on arrays of nanotubes to possibly obtain higher gains will be interesting.

ACKNOWLEDGMENTS

We thank Mu Chiao for access to wirebonder and Ali Kashefian for wirebonding the devices. Financial support was provided by the Natural Sciences and Engineering Research Council of Canada (NSERC) (Grant No. 341629-07) and the Canada Foundation for Innovation (CFI, Grant No. 13271). We also thank the Stanford University Beckman Cell Sciences Imaging Facility for their generous donation of the Philips 525M scanning electron microscope. M.M. also acknowledges support from the Bullitt Foundation.

APPENDIX: OXIDE-CHARGE CALCULATION

Oxide charging can be calculated as a function of the primary beam energy and current. The following equation can be used to calculate the charge left in the substrate (based on the model presented in Ref. 17):

$$I_B = \delta I_B + \eta I_B + I_{SC}, \tag{A1}$$

where I_B is the beam current and δ and η are the oxide secondary electron yield and backscattered electron yield coefficients, respectively, at the primary beam energy in use. I_{SC} is the leakage current due to the finite resistance of the dielectric, surface contamination, and electron-beam-induced currents that occur when the primary beam electrons penetrate beyond the dielectric layer. At low-beam energies the latter component is zero. As the substrate is bombarded with electrons some of them will be reflected due to elastic and inelastic collisions. Elastic collisions will generate backscattered electrons with energies ranging from 50 eV to the primary beam energy. Inelastic collisions occur between the primary beam electrons or backscattered electrons and the atoms of the dielectric and generate electrons with less than 50 eV (secondaries). The majority of reflected electrons will be of this type. The reflected electron yield, which is the sum of secondary and backscattered electron yields, is a function of the primary beam energy and the tilt of the sample. This yield will be equal to unity at two beam energies. For a beam normal to the sample these energies are less than 400 eV and approximately 3 keV for silicon dioxide (we call them E_1 and E_2, respectively).[17,19,20] For energies between E_1 and E_2 the reflected electron yield is larger than unity and everywhere else it is less than unity.

At the primary beam energies used in our experiments (3 keV or more) the yield is less than unity and some extra electrons will be left in the substrate, charging it negatively. This charge, however, will, in turn, raise the surface energy, $E_{surface}$, reducing the effective landing energy E of the primary beam electrons. The increased surface potential will also cause an increase in the leakage current through the oxide. The following equation can be used to calculate $E_{surface}$ and the landing energy E':[17]

$$E_{surface} = \frac{I_B R f_0 (E_0 - E_2)}{(E_0 - E_2) + I_B R f_0}. \tag{A2}$$

The landing energy is $E' = E_0 - E_{surface}$ and E_0 is the primary beam energy. The charging coefficient is $f_0 = 1 - (\delta + \eta)_{E'}$ and R is the bulk resistance, which is a function of the volume of all the current paths in the SiO_2. From the landing energy E' the substrate charging can be calculated using the secondary and backscattered yield coefficients at this energy and using Eq. (A1). We implemented the above equations to calculate the substrate charging with a MATLAB script using the SiO_2 backscattered and secondary electron yield coefficients published by Joy.[18] The values of yield coefficients not published in Joy's database were linearly interpolated.

---

*Corresponding author; anojeh@ece.ubc.ca

[1] L. A. Chernozatonskii, Y. V. Gulyaev, Z. J. Kosakovskaja, N. I. Sinitsyn, G. V. Torgashov, Y. F. Zakharchenko, E. A. Fedorov, and V. P. Val'chuk, Chem. Phys. Lett. **233**, 63 (1995).

[2] W. A. de Heer, A. Châtelain, and D. Ugarte, Science **270**, 1179 (1995).

[3] A. G. Rinzler, J. H. Hafner, P. Nikolaev, P. Nordlander, D. T. Colbert, R. E. Smalley, L. Lou, S. G. Kim, and D. Tománek, Science **269**, 1550 (1995).

[4] J.-M. Bonard, T. Stöckli, O. Noury, and A. Châtelain, Appl. Phys. Lett. **78**, 2775 (2001).

[5] Y. Saito and S. Uemura, Carbon **38**, 169 (2000).

[6] J.-M. Bonard, H. Kind, T. Stöckli, and L.-O. Nilsson, Solid-State Electron. **45**, 893 (2001).

[7] N. de Jonge, *Advances in Imaging and Electron Physics* (Elsevier, Maryland, Missouri, 2009), Vol. 156, pp. 203–233.

[8] P. Yaghoobi and A. Nojeh, Mod. Phys. Lett. B **21**, 1807 (2007).

[9] A. Nojeh, W.-K. Wong, A. W. Baum, R. F. Pease, and H. Dai, Appl. Phys. Lett. **85**, 112 (2004).

[10] A. Nojeh, W.-K. Wong, E. Yieh, R. F. Pease, and H. Dai, J. Vac. Sci. Technol. B **22**, 3124 (2004).

[11] C.-D. Kim *et al.*, Nanotechnology **17**, 5180 (2006).

[12] A. Nojeh, B. Shan, K. Cho, and R. F. W. Pease, Phys. Rev. Lett. **96**, 056802 (2006).

[13] E. Pop, D. A. Mann, K. E. Goodson, and H. Dai, J. Appl. Phys. **101**, 093710 (2007).

[14] C. Adessi and M. Devel, Phys. Rev. B **65**, 075418 (2002).

[15] G. C. Kokkorakis, A. Modinos, and J. P. Xanthakis, J. Appl. Phys. **91**, 4580 (2002).

[16] D. Drouin *et al.*, Scanning **29**, 92 (2007).

[17] H. Seiler, J. Appl. Phys. **54**, R1 (1983).

[18] D. C. Joy, 2008, http://web.utk.edu/srcutk/htm/interact.htm

[19] D. C. Joy and C. S. Joy, Micron **27**, 247 (1996).

[20] L. Reimer, *Image Formation in Low Voltage Electron Microscopy* (SPIE, Bellingham, WA, 1993).

[21] Y. A. Kasumov, I. I. Khodos, M. Kociak, and A. Y. Kasumov, Appl. Phys. Lett. **89**, 013120 (2006).

[22] A. Maiti, J. Andzelm, N. Tanpipat, and P. von Allmen, Phys. Rev. Lett. **87**, 155502 (2001).

[23] K. A. Dean, P. von Allmen, and B. R. Chalamala, J. Vac. Sci. Technol. B **17**, 1959 (1999).

[24] A. V. Krasheninnikov and F. Banhart, Nat. Mater. **6**, 723 (2007).